PAGEOPH, Vol. 145, Nos. 3/4 (1995) 0033-4553/95/040561-17$1.50 + 0.20/0

Oblique Subduction of a Newtonian Fluid Slab

ZHENG-KANG SHEN[1]

Abstract—A Newtonian fluid model is proposed to describe the oblique subduction of a planar 2-D slab. The slab is assumed to subduct in response to the ridge push force exerted along the trench, the slab pull force at the downdip of the slab, the gravitational body force within the slab, and the frictional resistance force at the upper surface of the slab. Because the slab motion along strike is being resisted by the frictional resistance at the interplate coupling area while the slab motion along the trench normal is being maintained by the gravitational pulling, the slab turns gradually toward the trench normal direction as it subducts. This model offers an alternative explanation for "earthquake slip partitioning," the observation that the earthquake slip vectors deflect away from the relative plate motion direction toward the trench normal direction along most of the oblique subduction zones worldwide. Numerical models suggest that slip partitioning caused by slab deformation could be as much as 30% at 100 km downdip of the slab. The slab viscosity, the plate coupling width, the interplate resistance coefficient, the slab pull force, and the gravitational body force are all important in determining the geometry of the slab subduction.

Key words: Oblique subduction, Newtonian fluid slab, earthquake slip partitioning.

Introduction

Oblique subduction exists at most of the subduction zones worldwide where the subducting plate thrusts obliquely under the overlying plate. Mechanical models have been developed to describe normal subduction (e.g., HAGER and O'CONNELL, 1978; TURCOTTE and SCHUBERT, 1982); however, important questions for oblique subduction remain to be answered. For example, could the oblique of a downgoing slab change during its subduction? If the answer is yes, what would be the controlling factors that would cause such deflection and by how much? Although considerable progress has been made in recent years in developing 3-D global mantle convection models using constraints from the geoid, plate velocity, and seismic tomography data (e.g., HAGER *et al.*, 1985; FORTE, and PELTIER, 1987; RICHARD and VIGNY, 1989; HAGER and CLAYTON, 1989; CADEK *et al.*, 1993), these models usually provide only convection patterns of very large scale (thousands of kilometers) and sparse detail about the trajectories of subducting slabs.

---

[1] Department of Earth and Space Sciences, University of California, Los Angeles, CA 90024-1567, U.S.A.

In this study a simple Newtonian fluid model is proposed to describe the updip portion of a subduction slab. This 2-D slab extends further along the trench parallel direction than along the downdip direction, and is subject to four major forces: the ridge push force applied along its top edge at the trench, the slab pull force at its downdip, frictional resistance at the interface between the downgoing slab and the upper plate, and the gravitational body force caused by excess density inside the slab. Because the degree of plate coupling is correlated with the plate subduction rate (RUFF and KANAMORI, 1980), we assume that the frictional resistance at the interplate surface is proportional to the plate motion velocity. If we assume that the viscosity and the frictional coefficient do not change with depth, this problem can be solved analytically.

This proposed oblique subduction model provides another way to examine the mechanism of earthquake slip partitioning. It has been observed that for most oblique subduction zones, slip directions of interplate subduction zone earthquakes tend to fall between the relative plate motion direction and the trench normal direction. Such deflection of the earthquake slip vector from the relative plate motion is called slip partitioning (FITCH, 1972). If the earthquake slip vectors reflect the local relative motion between the upper and lower plates, the missing part of the relative plate motion must take place somewhere else in the plates. This is usually explained by deformation in the upper plate (DEWEY, 1980; JARRARD, 1986; MICHAEL, 1990). One such model proposed by BECK (1983, 1991) and MCCAFFREY (1991, 1992, 1993) considered that part of the relative plate motion was accommodated by shear motion along a fault at the back of a silver plate located above the seismogenic zone of the subducting plate. In contrast, YU *et al.* (1993) proposed backarc spreading as a leading cause of the slip partitioning. PLATT (1993) developed a series of mechanical models to explain upper plate deformation caused by oblique subduction. Recently however, LIU *et al.* (1995) proposed deformation within the subducting slab as one of the important contributors to slip partitioning. They investigated the Circum-Pacific subduction zone earthquakes and found correlations between the earthquake slip partitioning and the calculated slab pull force. Their results suggested that the downgoing slab may be torqued by the slab pull and the frictional resistance at the interplate surface, causing the slab subduction direction to rotate.

This study, from the mechanical modeling point of view facilitates the answer to the question: can deformation of the descending slab be an important factor controlling the earthquake slip partitioning?

Mechanical Assumptions

The following assumptions are considered in the mechanical modeling:

1. The subducting slab is a 2-D planar plate, with a uniform thickness H. No plate bending is considered, and deformation associated with the curvature of a spherical earth surface is neglected.

2. The slab is a Newtonian fluid. The elastic effect of the slab is not considered because strains caused by such an effect would usually be two orders of magnitude smaller than the strains caused by the viscous effect during the subduction process.
3. Slab deformation in the direction normal to the plate surface is small and can be neglected. The stresses and the strain rates in the slab can be approximated by their respective averages over the thickness of the slab.
4. Three external forces are applied at the slab boundaries: the ridge push exerted at the upper boundary, the slab at the lower boundary, and the shear resistance at the interface between the slab pull and the upper plate. The mantle resistance between the lower surface of the slab and the upper mantle, significant or not, could also be included as part of the interface resistance. Outside the slab, hydrostatic equilibrium pressure is assumed. The slab is also being pulled internally by the gravitational body force resulting from the excess density within the slab. The slab extends further along the trench strike than along the downdip direction, and the forces at the two lateral boundaries of the slab are negligible.
5. The plate motion is considered on a geological time scale, so that episodic variations of plate velocities and stresses, which are on a time scale of about hundreds of years, are smoothed out; only the long-term averages of these physical properties are important and are assumed to be in a steady state.
6. The upper plate is stationary. The interface resistance is proportional to the slab velocity relative to the upper plate. The resistance coefficient and the viscosity of the slab remain constant throughout the entire slab.

Force Balance Equations

We consider the subducting slab moving at a steady velocity $\vec{U}$ and under stresses σ_{ij}. Figure 1 shows the setting of a plunging slab, with the $z = 0$ plane coinciding with the slab surface, the $y = 0$ plane at the downdip boundary between the interplate coupling and decoupling, the $y = L$ plane at the earth's surface, and the $z = -H$ plane at the lower surface of the slab. For a Newtonian fluid the force balance equations are (CHUNG, 1988)

$$-\rho U_{i,t} - \rho U_{i,j} U_j - p_{,i} + \lambda U_{j,ij} + \mu(U_{i,jj} + U_{j,ij}) + X_i = 0 \tag{1}$$

where U_i is the slab velocity, $i, j = x, y$, ρ is the density, p the hydrostatic pressure, X_i the body force, $\vec{X} = \rho\vec{g}$, and μ and λ are the first and second viscosity coefficients, respectively. The first term on the left-hand side vanishes for steady flow. The second term is several orders of magnitude smaller than the other terms and can be neglected.

Based on our third assumption, we can integrate Equation (1) from $z = -H$ to $z = 0$, and take the average of each term over the thickness of the slab. Outside the

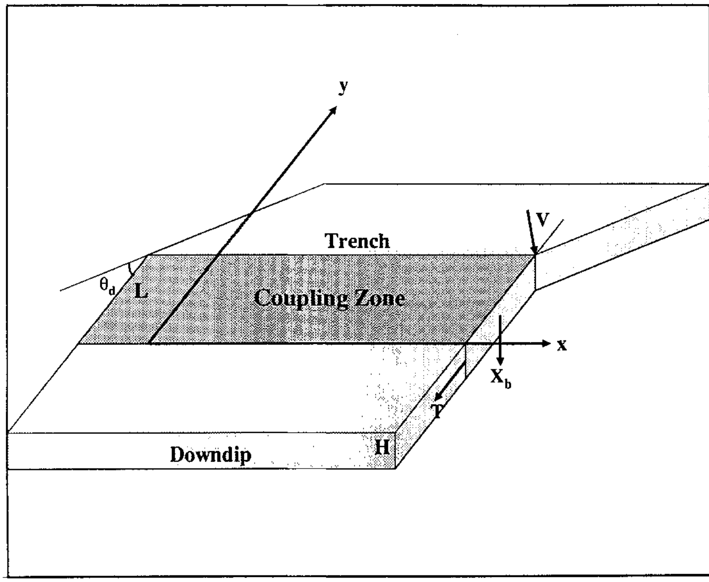

Figure 1
Model setting of a subducting slab. The plate has a uniform thickness H, the dark grey area denotes the interplate coupling zone of width L within the updip of the plate. The x axis is along the trench strike, the y axis along the updip, $z = 0$ is the plane of the interplate surface, and the $y = 0$ plane denotes the boundary of interplate coupling/decoupling. The slab dips at an angle θ_d, and is being pulled externally by a slab pull force T at the boundary cross section of $y = 0$, and internally by a gravitational body force of X_b. The slab velocity at the earth's surface before subduction is $\vec{V}$.

slab the pressure is under hydrostatic equilibrium $\rho_0 gh$. ρ_0 is the density outside the slab and h the depth measured from the surface of the earth. At the upper and lower boundaries of the slab, $p_{,x} = 0$ because the pressure has no gradient along x, and $p_{,y} = \rho_0 \sin\theta_d$. θ_d is the dip angle of the slab. Integrating of $p_{,y}$ over z yields $\bar{p}_{,y}H$, where $\bar{p}_{,y}$ is the mean pressure derivative with respect to y. $\bar{p}_{,y} = g\ \rho_0 \sin\theta_d$ if we assume that the mean of the pressure derivative approximately equals the pressure derivatives at the upper and lower surfaces of the slab.

Let u_i be the mean velocity U_i over z. The integration of the velocity terms in Equation (1) over z yields $\lambda u_{j,ij}H + \mu(u_{i,jj} + u_{j,ij})H - cu_i$, where $i, j = x, y$. The last term cu_i derives from the shear resistance due to coupling at the interface between the slab and the upper plate as stated in assumption No. 6, where c is the resistance coefficient at the interplate surface.

With all aforementioned developments considered, Equation (1) becomes:

$$\lambda u_{j,ij} + \mu(u_{i,jj} + u_{j,ij}) - \frac{c}{H}u_i - \Delta\rho g \sin\theta_d\,\delta_{iy} = 0 \qquad (2)$$

where $\Delta\rho = \rho - \rho_0$.

The velocity field can be generated by two potential functions Φ and A

$$\vec{u} = \nabla\Phi + \nabla \times A\hat{k}. \tag{3}$$

For a compressible slab, the force balance equations can be satisfied if the two potential functions satisfy the following equations

$$\nabla^2\Phi - \frac{1}{\alpha^2}\Phi - X'y = 0 \tag{4}$$

$$\nabla^2 A - \frac{1}{\beta^2}A = 0 \tag{5}$$

where $\alpha^2 = (\lambda + 2\mu)H/c$, $\beta^2 = \mu H/c$, and $X' = \Delta\rho g \sin\theta_d/\lambda + 2\mu$.

If the fluid is incompressible, a similar derivation yields

$$\nabla^2\Phi = 0 \tag{4'}$$

$$\nabla^2 A - \frac{1}{\beta^2}A - \frac{X}{c}x = 0. \tag{5'}$$

For the 2-D problem we are dealing with here, incompressible fluids sometimes lack solutions for arbitrary boundary conditions.

Let us assume the fluid is compressible. To have one more constraint on the viscous fluid, we assume the fluid obeys the Stokes' hypothesis, i.e., $\lambda = -2/3\mu$. This assumption is widely accepted for the real earth (RANALLI, 1987).

We introduce four boundary conditions for the problem, assuming we know the starting velocity at the upper boundary, and the stresses at the downdip of the interplate coupling. They are

$$\begin{aligned} u_x|_{y=L} &= F(x) \\ u_y|_{y=L} &= G(x) \\ \sigma_y|_{y=0} &= P(x) \\ \sigma_{xy}|_{y=0} &= Q(x). \end{aligned} \tag{6}$$

Let us first consider the simplest case of oblique subduction, i.e., that the obliquity and the subduction rate at the upper boundary are constant. We also assume a constant pulling force and zero shear at the downdip of the interplate coupling. The boundary conditions become

$$\begin{aligned} u_x|_{y=L} &= V_x \\ u_y|_{y=L} &= V_y \\ \sigma_y|_{y=0} &= T \\ \sigma_{xy}|_{y=0} &= 0. \end{aligned} \tag{7}$$

To solve the problem we consider the potential functions as the following

$$\Phi = \phi_c \cosh k_\phi y + \phi_s \sinh k_\phi y + \phi_y y \tag{8}$$

$$A = a_c \cosh k_a y + a_s \sinh k_a y. \tag{9}$$

From Equations (4), (5), (8), and (9), we obtain $k_\phi = 1/\alpha$, $k_a = 1/\beta$, and $\phi_y = -\Delta\rho g H \sin\theta_d/c$. The solution to the problem is thus

$$\begin{aligned}
\phi_c &= \frac{3}{4}\frac{T}{k_\phi^2 \mu H} \\
\phi_s &= \frac{V_y - \phi_y}{k_\phi \cosh k_\phi L} - \frac{3}{4}\frac{T \tanh k_\phi L}{k_\phi^2 \mu H} \\
a_c &= 0 \\
a_s &= \frac{V_x}{k_a \cosh k_a L}.
\end{aligned} \tag{10}$$

The corresponding velocity is

$$\begin{aligned}
u_x &= \frac{V_x}{\cosh k_a L}\cosh k_a y \\
u_y &= k_\phi(\phi_c \sinh k_\phi y + \phi_s \cosh k_\phi y) + \phi_y.
\end{aligned} \tag{11}$$

This solution shows that the along-strike velocity diminishes as subduction proceeds, and that the rate is determined by the constant of k_a. The along-dip velocity component is manifested by the combined effect of the gravitational body force, the slab pull at the lower end of the interplate coupling, and the shear resistance at the plate interface.

If the boundary conditions are more generic, we assume that they vary along the trench strike, and can be expressed by Fourier series, in the forms of

$$\begin{aligned}
F(x) &= \sum_n f_n \sin k_n x \\
G(x) &= \sum_n g_n \cos k_n x \\
P(x) &= \sum_n p_n \cos k_n x \\
Q(x) &= \sum_n q_n \sin k_n x.
\end{aligned} \tag{12}$$

The potential functions then become

$$\Phi = \sum_n (\phi_{nc} \cosh k_{\phi n} y + \phi_{ns} \sinh k_{\phi n} y)\cos k_n x + \phi_y y \tag{13}$$

$$A = \sum_n (a_{nc} \cosh k_{an} y + a_{ns} \sinh k_{an} y)\sin k_n x. \tag{14}$$

From Equations (4), (5), (13), and (14), we obtain $k_{\phi n} = \sqrt{k_n^2 + (1/\alpha^2)}$, $k_{an} = \sqrt{k_n^2 + (1/\beta^2)}$, and $\phi_y = -\Delta\rho g H \sin\theta_d/c$.

The boundary conditions require

$$
\begin{aligned}
\left(\frac{\partial \Phi}{\partial x}+\frac{\partial A}{\partial y}\right)\bigg|_{y=L} &= F(x) \\
\left(\frac{\partial \Phi}{\partial y}-\frac{\partial A}{\partial x}\right)\bigg|_{y=L} &= G(x) \\
\frac{2}{3}\mu\left(2\frac{\partial^2 \Phi}{\partial y^2}-\frac{\partial^2 \Phi}{\partial x^2}-3\frac{\partial^2 A}{\partial x\,\partial y}\right)\bigg|_{y=0} &= P(x) \\
\mu\left(2\frac{\partial^2 \Phi}{\partial x\,\partial y}-\frac{\partial^2 A}{\partial x^2}+\frac{\partial^2 A}{\partial y^2}\right)\bigg|_{y=0} &= Q(x).
\end{aligned}
\tag{15}
$$

From Equations (12), (13), (14), and (15), it is clear that for each n-*th* component we have four equations to solve for four unknowns ϕ_{nc}, ϕ_{ns}, a_{nc}, and a_{ns}.

Let us solve the problem with a specific set of boundary conditions. Assuming

$$
\begin{aligned}
u_x(x)|_{y=L} &= V \sin k_b x \\
u_y(x)|_{y=L} &= -V \cos k_b x \\
\sigma_y(x)|_{y=0} &= T \\
\sigma_{xy}(x)|_{y=0} &= 0
\end{aligned}
\tag{16}
$$

where V and T are constants. The first two boundary conditions define a constant velocity amplitude of the slab, with a varying obliquity of subduction at the trench where the subduction starts. These boundary conditions are approximately true for many subduction zones, such as the Aleutians, Tonga, and the New Hebrides, where the subduction directions vary monotonically by a large amount but the changes in velocity amplitudes are relatively small. The third boundary condition gives a constant slab pull force at the lower edge of the interplate coupling zone. The slab pull force is parallel to the y axis because the gravitational force has no component in the trench strike direction. If the slab pull force is a dominant force there, it should be close to one of the principal stresses, thus at the boundary where the slab pull applies, the shear stress should be close to zero, which is the fourth boundary condition.

Now all the equations in (15) are zero except two sets: $k_n = 0$ and $k_n = k_b$. These two sets of the equations become

$$
\begin{pmatrix}
0 & 0 & k_{a0}\sinh k_{a0}L & k_{a0}\cosh k_{a0}L \\
k_{\phi 0}\sinh k_{\phi 0}L & k_{\phi 0}\cosh k_{\phi 0}L & 0 & 0 \\
2k_{\phi 0}^2 & 0 & 0 & 0 \\
0 & 0 & k_{a0}^2 & 0
\end{pmatrix}
\begin{pmatrix}
\phi_{0c} \\ \phi_{0s} \\ a_{0c} \\ a_{0s}
\end{pmatrix}
=
\begin{pmatrix}
0 \\ -\phi_y \\ \dfrac{3}{2}\dfrac{T}{\mu H} \\ 0
\end{pmatrix}
\tag{17}
$$

and

$$\begin{pmatrix} -k_b \cosh k_{\phi s}L & -k_b \sinh k_{\phi s}L & k_{as} \sinh k_{as}L & k_b \cosh k_{as}L \\ k_{\phi s} \sinh k_{\phi s}L & -k_{\phi s} \cosh k_{\phi s}L & -k_b \cosh k_{as}L & -k_b \sinh k_{as}L \\ k_b^2 + 2k_{\phi s}^2 & 0 & 0 & -3k_b k_{as} \\ 0 & -2k_b k_{\phi s} & k_{as}^2 + k_b^2 & 0 \end{pmatrix} \begin{pmatrix} \phi_{bc} \\ \phi_{bs} \\ a_{bc} \\ a_{bs} \end{pmatrix} = \begin{pmatrix} V \\ -V \\ 0 \\ 0 \end{pmatrix} \tag{18}$$

The solutions to Equations (17) and (18) are

$$\begin{aligned} \phi_{0s} &= \frac{T}{c} \\ \phi_{0c} &= \frac{\Delta\rho g \sin\theta_d H}{c k_{\phi 0} \cosh k_{\phi 0} L} - \frac{T}{c} \tanh k_{\phi 0} L \\ a_{0c} &= 0 \\ a_{0s} &= 0 \\ \phi_{bc} &= \frac{V}{\Theta}\left(C_{22} + C_{12} - (C_{13} + C_{23})\frac{C_{42}}{C_{43}}\right) \\ \phi_{bs} &= \frac{V}{\Theta}\left(-(C_{11} + C_{21}) + (C_{14} + C_{24})\frac{C_{31}}{C_{34}}\right) \\ a_{bc} &= -\frac{C_{42}}{C_{43}}\phi_{bc} \\ a_{bs} &= -\frac{C_{31}}{C_{34}}\phi_{bc} \end{aligned} \tag{19}$$

where

$$\Theta = \left(C_{11} - C_{14}\frac{C_{31}}{C_{34}}\right)\left(C_{22} - C_{23}\frac{C_{42}}{C_{43}}\right) - \left(C_{12} - C_{13}\frac{C_{42}}{C_{43}}\right)\left(C_{21} - C_{23}\frac{C_{31}}{C_{34}}\right),$$

and C_{ij} are the components in the 4×4 matrix of Equation (18).

We numerically examine solutions using the parameters given in the following, which will be justified later. The slab interplate coupling width L is given as 200 km, slab thickness H is 60 km, the velocity amplitude at upper boundary V is 10 cm/yr, and its wave number k_b is $\pi/2000\ \text{km}^{-1}$. The viscosity μ is assumed to be 10^{22} Pa–s, the frictional coefficient c is taken as 1.8×10^{16} Pa–s/m, the gravitational body force $X_b = \Delta\rho g \sin\theta_d = 7.1 \times 10^2$ Pa/m, and slab pull at the lower boundary of the slab $T = 3.0 \times 10^{12}$ N/m. We label this set of parameters as the "preferred" model parameters. For a model with a constant upper boundary obliquity of 45% (Equation 11), Figure 2 delineates the subducting slab trajectory of the preferred

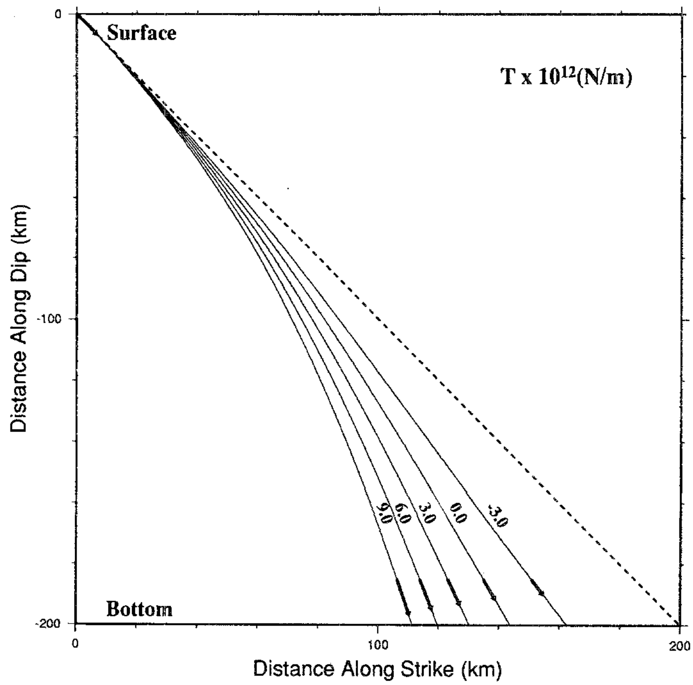

Figure 2
Slab trajectories predicted by models with a constant subduction obliquity at the earth's surface given by Equation (11). Subduction rates and directions are shown by arrows. The preferred model parameters are used in the models. Models with five different slab pull forces, ranging from -3.0 to 9.0×10^{12} N/m, are examined. The preferred model ($T = 3 \times 10^{12}$ N/m) predicts a nearly constant subduction rate, with oblique angles rotating gradually towards the trench normal.

model, as well as trajectories of the same model but different slab pull forces. Figure 3 supplies the velocity profile for the model of variable obliquity along trench strike (Equation 19).

If we assume a slab pull force of 3.0×10^{12} N/m, the constant and variable obliquity models given above describe the subduction process driven dominantly by the gravitational body force, which is offset mainly by the along-trench normal component of the shear resistance at the slab upper surface. Therefore, we see an almost constant velocity amplitude from top to bottom, with the obliquity angle rotating gradually toward trench normal. At the mid-point of the interplate coupling zone (100 km), the oblique angle is 59° for the constant obliquity model, which represents about a 30% deflection from its original 45° obliquity prior to subduction. Obliquity at 100 km downdip for the variable obliquity model has approximately 25% deflection. Both models suggest that the obliquity angle change occurs mostly in the upper part of the slab. While the reduction of the oblique angle could be 44% and 32% of the original value at the trench for the two models

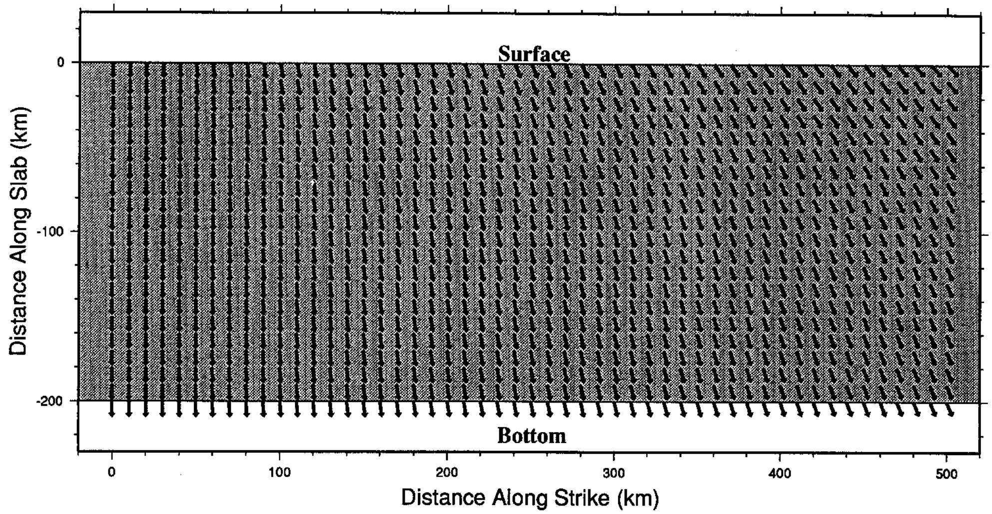

Figure 3

Velocity profile within the interplate coupling zone of a slab. This slab begins the subduction at the trench with a uniform rate and a monotonically increased obliquity along-trench strike given by the model of Equation (19). The preferred model parameters are used. Similar to the previous model of a constant obliquity along-trench strike (Eq. 11), this model predicts a nearly constant subduction rate, where the oblique angles rotate gradually towards the trench normal.

respectively after 200 km subduction, 30% and 25% of the reduction could be reached halfway through the process.

Model Justification

In the models given above we have made assumptions for several parameters. Some have well-known constraints, others do not. It is necessary to examine how the variations of those parameters would affect our models, and to assess reasonable ranges of the parameters. The following discussions are focused on the variations of the model with constant obliquity at earth's surface, since this model, although simple, is sufficient to test all the important parameters.

Slab Pull Force T

Figure 2 shows the effect of the slab pull force acting at the bottom of the interplate coupling zone on the trajectory of the slab as well as on the amplitude of the subduction rate. The slab is being stretched or compressed mostly at the bottom of the coupling zone, depending on the type and amount of the slab pull force exerted there. A negative slab pull reflects the resistance of the mantle material to the penetrating slab. Such resistance tends to push the slab velocity toward the trench strike direction, therefore reducing the degree of slip partitioning. Assuming the same density anomaly as we use in the preferred model, a slab pull force of 3.0×10^{12} N/m is equivalent to an accumulative gravitational pulling force inside the slab of about 72 km downdip. This estimate leads to the depth of a neutral downdip stress of about 190 km depth, consistent with the findings of ZHOU (1990) that most of the neutral downdip stress zones are located between 100 and 300 km depth in the NW Pacific and the Tonga-Kermadec subduction zones. The change of obliquity with respect to the slab pull force around this preferred model is about $0.9°/10^{12}$(N/m) at 100 km depth, or about 2% of its original oblique angle at the surface per 10^{12}(N/m) slab pull force increment.

Viscosity μ

Constraints on the viscosity of the lithosphere have been derived by studying the viscous responses of the earth to an external load, such as measuring the post-glacial rebound in Canada (PELTIER, 1980; WALCOTT, 1972, 1973). A model of a Newtonian mantle would require the viscosity to be in the range of $10^{21}-10^{22}$ Pa–s to explain the postglacial rebound data (RANALLI, 1987). The subducting slab however is colder therefore stronger than the mantle. KAULA (1980) estimated the lithosphere viscosity to be about 10^{22} Pa–s by analyzing the spherical harmonic spectra of plate velocities, gravity, topography, and heat flow data. We test the effects of different viscosity values on our model and present the results in Figure 4. If all the parameters coincide as in the previous model, and the viscosity is varied from 5×10^{21} Pa–s to 5×10^{22} Pa–s, then the results indicate that for higher viscosities the slab becomes stiffer, and exhibits less deflection of the oblique angle. Although both the subduction rates and the obliquities are affected, the effect of viscosity variation on the oblique angles is more significant. The degree of "partitioning," defined here as the ratio of the obliquity change at 100 km downdip over the original obliquity at the surface, increases from 8% to 47% as the viscosity decreases from 5×10^{22} Pa–s to 5×10^{21} Pa–s. The changes in the subduction rate are within 5% for the same range of viscosity variation. These results suggest that the plate subduction rate would not depend substantially on the viscosity, but the subduction direction would strongly depend on the viscosity.

Friction Coefficient c

FORSYTH and UYEDA (1975) estimated the relative strength of the plausible driving forces of plate motions. They postulated the relative ridge push per unit length along the strike to be $F_{rp} = 0.36$ and the relative slab resistance per unit

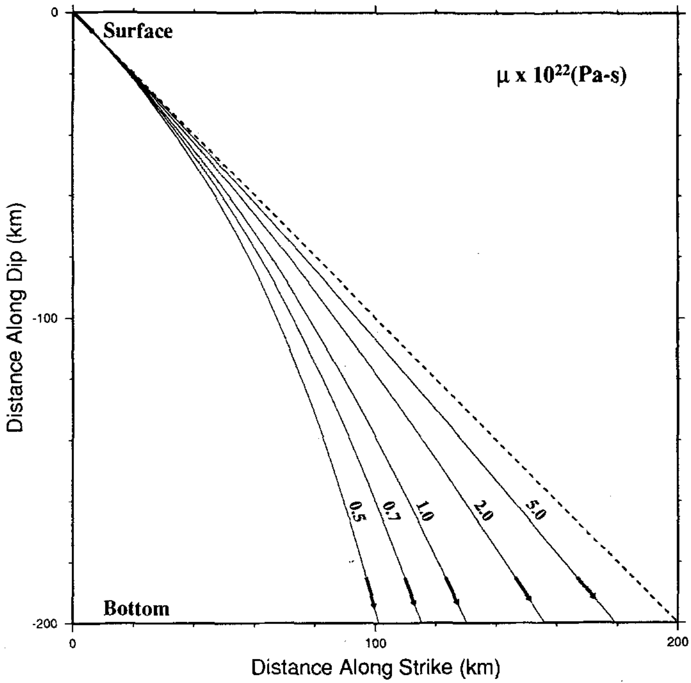

Figure 4
Slab trajectories predicted by models with different viscosity. The viscosity values tested are 0.5, 0.7, 1.0, 2.0, and 5.0. The remaining parameters are those of the preferred model. This result shows that the obliquity decreases following the decrease of the viscosity, corresponding to larger slip partitioning. The velocity amplitude changes are less significant than the changes in obliquity.

length along the strike and per plate motion velocity (cm/yr) to be $F_{sr} = 0.89$. Assuming the slab resistance at the subduction zone comes from the interplate resistance, we can write the ratio of the two forces as

$$\frac{F_{sr}}{F_{rp}} = \frac{cL}{\sigma_{rp} W} \tag{20}$$

where L is the length of the interplate coupling, W the thickness of the plate near the ridge, and σ_{rp} the ridge push stress. ARTYUSHKOV (1973) estimated σ_{rp} to be about 230 bars. If we assume $L = 2000$ km and $W = 30$ km, the friction coefficient c is then 1.8×10^{16} Pa–s/m. This value is obtained after rescaling the assumed plate motion velocity. Forsyth and Uyeda assumed 7 cm/yr for the velocity when deriving the relative strength ratio, while 10 cm/yr is assumed in this study. As FORSYTH and UYEDA (1975) pointed out, the values obtained by such studies are only orders of magnitude estimates, due to the uncertainties of their model as well as the uncertainties of data. We test the friction coefficient c at five different values, covering a broad range of 0.4×10^{16}–7.2×10^{16} Pa–s/m in Figure 5. Results show

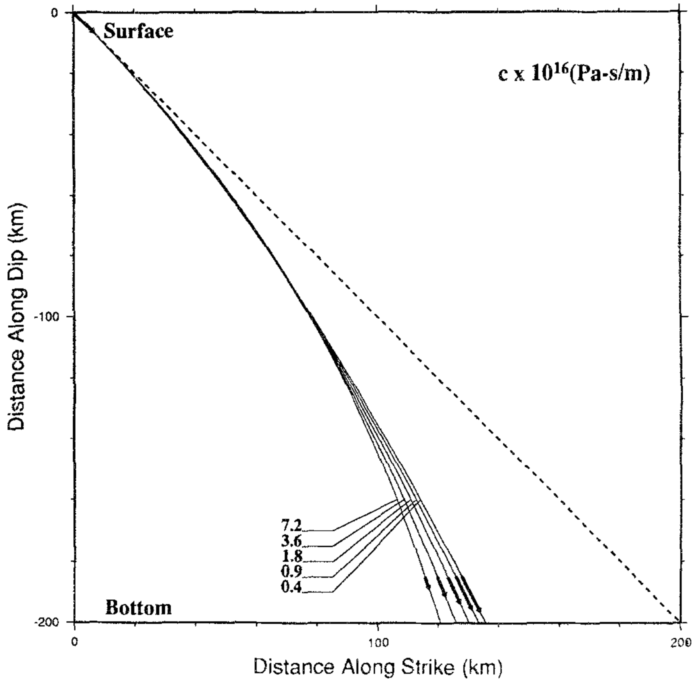

Figure 5
Slab trajectories predicted by models with different frictional resistance coefficient. The frictional resistance coefficient is assumed 0.4, 0.9, 1.8, 3.6, and 7.2×10^{16} Pa–s/m. The remaining parameters are those of the preferred model. A steady decrease of the subduction rate is found along with the increase of the frictional resistance. The oblique angle is also slightly decreased.

that the oblique angle and the subduction rate decrease as the friction coefficient increases. However, the obliquity of the subducting slab is much less sensitive to the friction coefficient than the subduction rate is.

Gravitational Body Force X_b

The subducted slab is colder than its surrounding mantle and therefore contains higher density. The density anomaly of the slab causes an extra gravitational pull within the slab. The density anomaly within a downgoing slab can be inferred from gravitational studies (GARLAND, 1979). A gravity anomaly study across the Japan Trench placed a 100 kg/m^3 density anomaly in the slab (HATHERTON, 1969). Similar values can also be obtained from mantle convection models. The excess density in a slab can be expressed as $\Delta\rho = \rho\alpha\,\Delta T$, where α is the coefficient of thermal expansion and ΔT the temperature difference inside and outside the slab. Using the values from TURCOTTE and SCHUBERT (1982), $\Delta\rho = 3.3 \times 10^3$ kg/m^3, $\alpha = 3 \times 10^{-5}$ °K^{-1}, and $\Delta T = 800$ °K, we estimate $\Delta\rho$ as

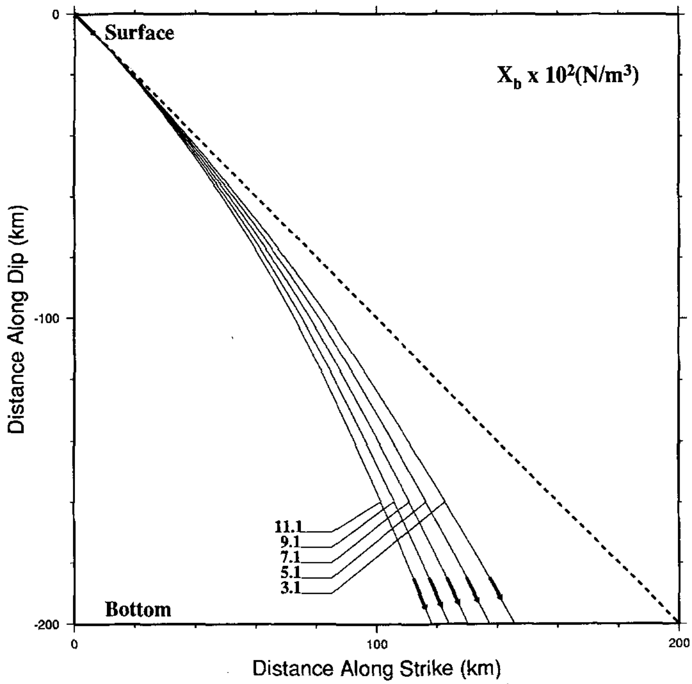

Figure 6
Slab trajectories predicted by models with different gravitational body force. The gravitational body force values are set at 3.1, 5.1, 7.1, 9.1, and 11.1 $\times 10^2$ N/m^3 while the remaining parameters are those of the preferred model. A steady decrease is found for the obliquity with a moderate increase of the subduction rate along with the increase of the gravitational body force.

about 80 kg/m^3, which is quite close to the value given by the gravitational study mentioned above. Although the results of such studies suffer from large uncertainties and are model dependent, it is believed that the density anomaly in a slab should be on the order of 100 kg/m^3. Figure 6 shows the testing of the effect of the gravitational body force on the subducting slab. As expected, greater body force yields a faster subduction rate and larger oblique angle deflection. The effect is significant for both of them.

Interplate Coupling Width L

The interplate coupling width L can vary region by region. The maximum width of seismic coupling derived from ruptures of great earthquakes is about 200 km (LAY *et al.*, 1982). However the shear resistance at the interplate surface is likely to exist beyond the seismic coupling zone, where the brittle coupling is replaced by the viscous traction. We test the coupling width effect on our model in Figure

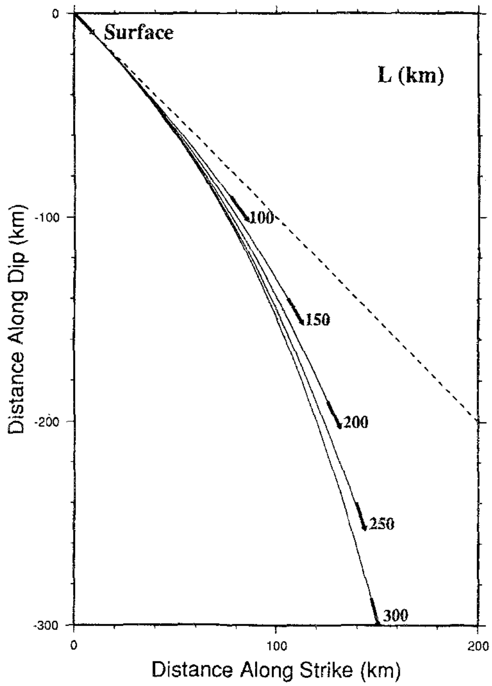

Figure 7
Slab trajectories predicted by models with different interplate coupling width. The interplate coupling width is assumed 100, 150, 200, 250, and 300 km while the remaining parameters are those of the preferred model. Both the oblique angle and the subduction rate are affected by the interplate coupling length. See text for more detailed discussions.

7. As can be seen, the deflection of the oblique angle is related to the width of the coupling zone. The longer the coupling zone is, the more lateral resistance exerted on the slab, and therefore the more slip partitioning. The obliquity changes from 53° to 61° at 100 km depth when the width of the coupling zone increases from 100 km to 300 km. This represents a change of about 19–35% from its original 45° obliquity at the earth's surface. The subduction rate shows negligible dependence on the coupling width.

The change of coupling width is correlated with the change of slab pull force in this study, because the point of slab pull force applied to is at the bottom of the coupling zone in our model. A longer coupling width basically moves the point of external slab pull downward. Such an effect could be tested by varying the slab pull force and the interplate coupling width simultaneously. However such tests would be complex and we choose to limit our test to a single parameter variation here. At the circumstances when slip partitioning is nearly complete at the bottom of the coupling zone, such effects could not be significant.

Discussion and Conclusions

Some tectonic features in the real earth are not being modeled in this study, such as temperature-dependent viscosity, forces generated by the curvature of the slab, and along-strike deformation of the upper plate caused by the shear of our obliquely subducted slab. These factors will somewhat affect the outcome of our model, especially the deformation of the upper plate, which might cause less deflection of the slab obliquity by reducing the lateral shear exerted on the surface of the slab. Despite these shortcomings, however, this model has the advantage of being a simple model, and it reveals some important features of an obliquely subducted slab.

In this study a Newtonian fluid is used to model an oblique subduction process. The slab is acted on by an internal gravitational body force, an external slab pull force at the downdip end, and a resistive shear force exerted at the interplate surface between the slab and the upper plate. The shear force reduces the obliquity of the subduction and makes the slab motion direction change gradually toward the trench normal. The reduction in obliquity is most effective when the obliquity is large, therefore the mechanism becomes a good candidate to explain earthquake slip partitioning at the upper part of the interplate coupling. In a model with reasonable parameter values, a 30% change of obliquity is observed halfway into the interplate coupling zone. The viscosity, the gravitational body force, the slab pull at downdip, the friction resistance coefficient, and the interplate coupling width all play important roles in controlling oblique subduction. A sizeable range of slip partitioning values could be obtained by varying model parameters still within their plausible ranges.

Acknowledgments

The author is grateful to Gerald Schubert, Leon Knopoff, David Jackson, and Xinping Liu for their valuable comments and suggestions. The author also thanks Peter Zwick, whose review helped to improve the manuscript. David Potter has read the revision of the manuscript and his comments are appreciated.

References

Artyushkov, K. V. (1973), *Stresses in the Lithosphere Caused by Crustal Thickness Inhomogeneities*, J. Geophys. Res. *78*, 7675–7708.

Beck, M. E., Jr. (1983), *On the Mechanism of Tectonic Transport in Zones of Oblique Subduction*, Tectonophysics *93*, 1–11.

Beck, M. E., Jr. (1991), *Coastwise Transport Reconsidered: Lateral Displacements in Oblique Subduction Zones, and Tectonic Consequences*, Phys. Earth Planet. Int. *68*, 1–8.

Cadek, O., Ricard, Y., Martinec, Z., and Matyska, C. (1993), *Comparison between Newtonian and Non-Newtonian Flow Driven by Internal Loads*, Geophys. J. Int. *112*, 103–114.

CHUNG, T. J., *Continuum Mechanics* (Prentice Hall, London 1988).

DEWEY, J. F. (1980), *Episodicity, Sequence and Style at Convergent Plate Boundaries, the Continental Crust and its Mineral Deposits*, Spec. Pap. Geol. Assoc Can. *20*, 553–573.

FITCH, T. J. (1972), *Plate Convergence, Transcurrent Faults and Internal Deformation of the Pacific Northwest Continental Margin*, Geology *19*, 978–981.

FORSYTH, D., and UYEDA, S. (1975), *On the Relative Importance of the Driving Forces of Plate Motion*, Geophys. J. R. Astr. Soc. *43*, 163–200.

FORTE, A. M., and PELTIER, W. R. (1987), *Plate Tectonics and Aspherical Earth Structure: The Importance of Poloidal-toroidal Coupling*, J. Geophys. Res. *92*, 3645–3679.

GARLAND, G. D., *Introduction to Geophysics* (W. B. Saunders Company, Philadelphia 1979).

HAGER, B. H., and O'CONNELL, R. J. (1978), *Subduction Zone Dip and Flow Driven by Plate Motions*, Tectonophysics *50*, 111–133.

HAGER, B. H., CLAYTON, R. W., RICHARDS, M. A., COMER, R. P., and DZIEWONSKI, A. M. (1985), *Lower Mantle Heterogeneity, Dynamic Topography and the Geoid*, Nature *313*, 541–545.

HAGER, B. H., and CLAYTON, R. W., *Constraints on the structure of mantle convection using seismic observations, flow models and the geoid, in mantle convection*. In *Plate Tectonics and Global Dynamics* (ed. Peltier, W. R.) (Gordon and Breach Scientific Publ., New York 1989).

JARRARD, R. D. (1986), *Relations among Subduction Parameters*, Rev. Geophys. *24*, 217–284.

HATHERTON, T. (1969), *Gravity and Seismicity of Asymmetric Active Regions, Nature 221*, 353.

KAULA, W. (1980), *Material Properties for Mantle Convection Consistent with Observed Surface Fields*, J. Geophys. Res. *85*, 7031–7044.

LAY, T., KANAMORI, H., and RUFF, L. (1982), *The Asperity Model and the Nature of Large Subduction Zone Earthquakes*, Earthq. Pred. Res. *1*, 3–72.

LIU, X., MCNALLY, K., and SHEN, Z. (1995), *Evidence for a Role of the Downgoing Slab in Earthquake Slip Partitioning at Oblique Subduction Zones*, J. Geophys. Res., in press.

MCCAFFREY, R. (1991), *Slip Vectors and Stretching of the Sumatran Forearc*, Geology *19*, 881–884.

MCCAFFREY, R. (1992), *Oblique Plate Convergence, Slip Vectors, and Forearc Deformation*, J. Geophys. Res. *97*, 8905–8915.

MCCAFFREY, R. (1993), *Global Variability in Subduction Thrust Zone-forearc Systems*, Pure and Appl. Geophys. *140*, 1–52.

MICHAEL, A. J. (1990), *Energy Constraints on Kinematic Models of Oblique Faulting: Loma Prieta versus Parkfield-Coalinga*, Geophys. Res. Lett. *17*, 1453–1456.

PELTIER, W. R., *Mantle Convection and Viscosity*, In *Physics of the Earth's Interior* (eds. Dziewonski, A. M., and Boschi, E.) (North Holland Publ., Amsterdam 1980) pp. 362–431.

PLATT, J. P. (1993), *Mechanics of Oblique Convergence*, J. Geophys. Res. *98*. 16239–16256.

RANALLI, G., *Rheology of the Earth* (Allen and Unwin Inc., Winchester, Mass. 1987).

RICARD, Y., and VIGNY, C. (1989), *Mantle Dynamics with Induced Plate Tectonics*, J. Geophys. Res. *94*, 17543–17559.

RUFF, L., and KANAMORI, H. (1980), *Seismicity and the Subduction Process*, Phys. Earth. Planet. Int. *23*, 240–252.

TURCOTTE, D. L., and SCHUBERT, G., *Geodynamics Applications of Continuum Physics to Geological Problems* (John Wiley and Sons, New York 1982).

WALCOTT, T. I. (1972), *Late Quaternary Vertical Movements in Eastern North America: Quantitative Evidence for Glacio-isostatic Rebound*, Rev. Geophys. Space Phys. *10*, 849–884.

WALCOTT, T. I. (1973), *Structure of the Earth from Glacio-isostatic Rebound*, Ann. Rev. Earth and Planet. Sci. *1*, 15–37.

YU, G., WESNOUSKY, S. G., and EKSTRÖM, G. (1993), *Slip Partitioning along Major Convergent Plate Boundaries*, Pure and Appl. Geophys. *140*, 183–210.

ZHOU, H.-W. (1990), *Observations on Earthquake Stress Axes and Seismic Morphology of Deep Slabs*, Geophys. J. Int. *103*, 377–401.

(Received October 15, 1994, revised March 27, 1995, accepted April 5, 1995)